Transmission Loss Optimization-Based Optimal Power Flow Strategy by Hierarchical Control for DC Microgrids

Junchao Ma, *Student Member, IEEE*, Liqiang Yuan, *Member, IEEE*, Zhengming Zhao, *Senior Member, IEEE*, and Fanbo He, *Member, IEEE*

***Abstract*—This paper proposes an efficient power flow sharing and voltage regulation control method based on hierarchical control to minimize the transmission loss of dc microgrids. Different from the conventional optimal power flow algorithm for the dc grids, the proposed approach needs neither prior knowledge of the grid's conductance matrix nor the load distribution matrix, which means improvement of the expansibility and reduction of the cost. At the primary control level, a voltage droop characteristic is set for each converter to improve the stability and reliability of the grid. The secondary control level aims to regulate the power flow of the microgrid to the optimal condition. The two control levels exchange information by low bandwidth communication. The validity of the proposed approach is verified by both simulation results of a dc microgrid based on IEEE 14-bus system and experimental results on a 50-V two-terminal prototype dc microgrid.**

***Index Terms*—DC microgrids, hierarchical control, optimal power flow (OPF), transmission loss optimization.**

I. Introduction

THE increasing penetration of distributed energy resources with dc power such as solar photovoltaic and energy storage systems as well as the growth of dc loads such as data centers and LED lighting applications has attracted more and more attention on the utilization of dc power in electric systems and microgrids.

With a higher penetration of power electronics converters in dc microgrids, it is a common conclusion that the conversion and transmission efficiency is a shortcoming of dc grids comparing with ac grids especially in short-distance and low-voltage networks. To reduce the transmission power loss, optimal power flow (OPF) is an efficient way. The idea of OPF was proposed decades of years ago. Minimizing the line losses of the utility grid by regulating the power flow is the basic idea of OPF. Ever since it was put forward, the OPF strategy commonly needs the entire knowledge of the grid structure, line impedance, and load distribution, which limits the technique to the utility grid or grids whose architecture is relatively fixed. In recent years, with the rising up of dc technology, research on OPF for dc grids [1], [2], [16], [17] or ac/dc hybrid grids [3], [18]–[20] has been conducted. Most of these efforts focused on HVdc or MTDC and the OPF strategy is still based on the optimization algorithm in ac grids. As stated in [2], "the optimal dc-power flow (dc-OPF) algorithm can be simply copied from the available OPF algorithms for the ac-power system, considering some slight modifications," which means the dc-OPF algorithm still depends on the grid information such as grid's conductance matrix (GCM) and load distribution matrix (LDM) like ac-OPF.

On the other hand, OPF for low-voltage grids, such as distribution networks or microgrids, is less common. For microgrids, economic efficiency and expansibility are especially sensitive which makes a big challenge for the OPF strategy in microgrids. Another challenge is that in microgrids, power sources and loads may have frequent reconfigurations in the grid architecture. These characteristics of dc microgrids make the grid information which the conventional dc-OPF algorithm depends on hardly available. In [4], an OPF strategy for ac microgrids without significant communication or architecture information was proposed. The proposed method in [4] was like the perturbation and observation algorithm in MPPT of solar generation. Though the feasibility of the method was verified by simulation in [4], the simulation is too simple with only four nodes in the network and it is not verified with experiments. Whether the method is still effective in a complex network is doubted. In conclusion, an effective OPF strategy which does not depends on the GCM and LDM is needed in dc microgrids.

Hierarchical control structure is commonly applied to all kinds of electronic grids [5], [6], [21], especially in microgrids. Hierarchical control is an efficient way to endow smartness and flexibility to microgrids [5]. Much research on dc-OPF for HVdc or MTDC is also based on hierarchical control [1], [2], [19]. For dc microgrids, the basic function of the conventional hierarchical control is to restore the voltage deviations produced by the distributed droop control [5], [7]–[13]. Later research on hierarchical control application in dc microgrids mostly focuses on the management of the storage system [8], [10], [12], [15] or current flow sharing accuracy [13]. Battery management is important for increasing the efficiency and lifetime of the storage system [12], but it helps a little in increasing the entire efficiency of the microgrid system. In the low-voltage distribution, the transmission loss may reach 5%–8%. Investigations on HVdc and MTDC have proved that proper OPF algorithm based on hierarchical control may cut off half of the transmission

Manuscript received November 24, 2015; revised March 7, 2016; accepted April 18, 2016. Date of publication May 4, 2016; date of current version December 9, 2016. This work was supported by the Major Program of the National Natural Science Foundation of China (51490683). Recommended for publication by Associate Editor J. M. Guerrero.

The authors are with the State Key Laboratory of Power System, Department of Electrical Engineering, Tsinghua University, Beijing 100084, China (e-mail: majc11@mails.tsinghua.edu.cn; ylq@tsinghua.edu.cn; zhaozm@tsinghua.edu.cn; hefanbo@gmail.com).

Color versions of one or more of the figures in this paper are available online at http://ieeexplore.ieee.org.

Digital Object Identifier 10.1109/TPEL.2016.2561301

losses [1], [2], which is a prominent improvement in the grid efficiency.

Different from HVdc or MTDC, in a dc microgrid, the definition of power supply source and load node is not quite distinct, so it is important to make it clear. As we focus on the OPF strategy, the distinction between the power source and the load here is not based on the direction of power flow. Only the grid nodes whose output (or input) power can be regulated (controllable sources) are defined as power supply sources. This means only nodes such as storage systems, V2G EVs, PCC nodes, etc., can be considered as power supply nodes. It is not recommended to sacrifice the MPPT efficiency of the distributed renewable energy generation systems (uncontrollable sources) and regulate the output of those nodes for OPF. Thus, renewable energy nodes, conventional loads, EVs without the V2G mode, are all treated as loads in the proposed OPF strategy.

In this paper, an OPF strategy which does not depend on the prior knowledge of the grid information (GCM and LDM) based on the hierarchical control framework for dc microgrids with the generic structure is proposed. The OPF condition in dc microgrids with generic structure is derived in Section II. A control strategy for the OPF condition realization in dc microgrids is shown in Section III. Case study and simulation results of the proposed OPF realization method are shown in Section IV and the experimental results are offered in Section V.

II. Optimal Condition Derivation

A. Transmission Loss Modeling of Generic DC Microgrids

A generic dc microgrid with X power source nodes, whose architecture is discretional, is considered in the derivation. To start the derivation, a power supply node a is chosen randomly. Suppose that node a is connected to other $m-1$ power supply nodes, namely $b, c, \ldots, m$, which is shown in Fig. 1(a). The details of the branch from a to b is highlighted in Fig. 1(b) as an example.

Some assumptions are presented as follows.

1) The line impedance can be simplified as resistance, since the grid is dc supplied;
2) each power supply node is connected to the grid through voltage-source converters (VSC) whose output voltage can be regulated;
3) all loads are considered to be current-source loads which is a common processing mode in OPF condition derivation.

Commonly, the transmission loss contains two parts, namely the line loss Pl_{line} and the converter loss Pl_{conv}. The converter loss can be simplified as a quadratic expression of the output current shown as [3], [14]

$$Pl_{\text{conv}} = f(i) = ai^2 + b|i| + c. \tag{1}$$

With the approximate model of the converter loss as (1), the gross transmission losses of the grid can be derived as

$$\begin{cases} Pl = Pl_{\text{conv}} + Pl_{\text{line}} \\ Pl_{\text{conv}} = \sum Pl_{\text{conv}(x)} = \sum f_x(i_x) \quad x, y = a, b, \ldots, m \\ Pl_{\text{line}} = \sum Pl_{\text{line(xy)}} = \sum i_{\text{xy}}^2 R_{\text{xy}}, \end{cases} \tag{2}$$

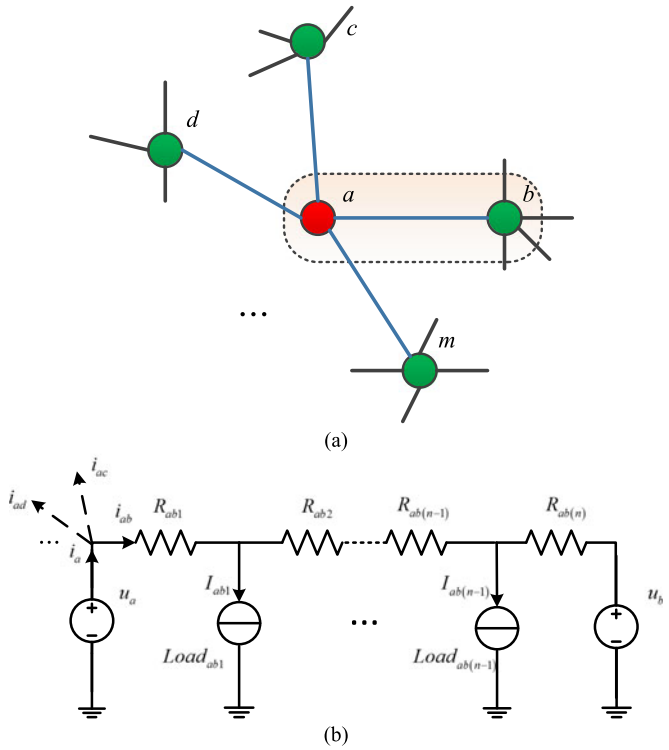

Fig. 1. Circuit model of a dc microgrid with geneic grid structure. (a) Brief view of the dc microgrid from power supply node a with only power supply nodes. (b) Branch from a to b, which shows the details of the highlighted part in (a).

where $Pl_{\text{conv}(x)}$ is the conversion loss of power supply node x ($x = a, b, \ldots, m, \ldots, N$), and $Pl_{\text{line}(xy)}$ is the line loss of the branch x-y ($x, y = a, b, \ldots, m, \ldots, N$).

B. Derivation of the OPF Condition With One Power Supply Node Controllable

As analyzed, only power supply nodes are controllable for the OPF algorithm, so the OPF condition of a dc microgrid actually refers to the optimized operation states of all the power supply nodes. However, it is difficult to take all the X power supply nodes into consideration at the same time directly. So instead of deriving the OPF condition of a generic dc microgrid directly, the first step here is to derive the OPF condition with the assumption that only one power supply is controllable for the OPF algorithm in a generic structured dc microgrid.

As Fig. 1, power supply node a is randomly chosen for the first step of the derivation, which means only output voltage of power supply node a is supposed to be controllable in the following derivation. As all the power supply nodes are supposed to be connected to the grid with VSC, they are constant-voltage sources in the derivation. How the transmission loss changes with the output voltage of node a is derived as follows.

As Fig. 1(b) shows the equivalent circuit of a certain branch can be regarded as a two-port nonlinear time-invariant network with two power supply sources as inputs whose output voltage can be regulated (shown as Fig. 2). Therefore, the currents and voltages in the network are only decided by the input voltages

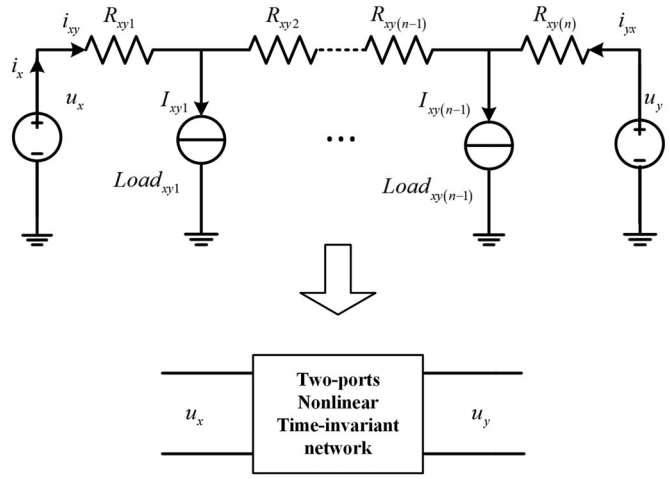

Fig. 2. Two-port equivalent circuit of a branch *x*-*y* in dc microgrids.

of the two ports, which means as long as u_x and u_y are kept constant, the voltage variation of another power supply source will not influence the currents or voltages in branch *x*-*y*.

As in this part, we assume that only the output voltage of power supply node *a* can be regulated, it is clear that the variation of u_a can only influence the power flow on the branches that is directly connected to *a* (the blue branches in Fig. 1), which also means the change of u_a can only influence the line losses on those branches (*a*-*b*, *a*-*c*, . . . , *a*-*m*) and the converter losses of *a*, *b*, *c*, . . . , *m*. Thus, the transmission loss optimization problem of the whole grid as (2) can be drawn as

$$\begin{cases} \min \quad Pl = Pl_{\text{conv}} + Pl_{\text{line}} \\ Pl_{\text{conv}} = Pl_{\text{conv}(a)} + Pl_{\text{conv}(b)} + \ldots + Pl_{\text{conv}(m)} + C_1 \\ Pl_{\text{line}} = Pl_{\text{line(ab)}} + Pl_{\text{line(ac)}} + \ldots + Pl_{\text{line(am)}} + C_2 \end{cases} \tag{3}$$

where C_1 is the constant part in Pl_{conv} containing the converter losses of power supply nodes other than *a*, *b*, *c*, . . . , *m*, and C_2 is the constant part in Pl_{line} containing the line losses in branches not directly connected to *a*.

From Fig. 1 and (2), the converter loss is modeled as

$$Pl_{\text{conv}(x)} = f_x\left(i_x\right) \quad x = b, c, \ldots, m\,. \tag{4}$$

As analyzed in Section II-A, the variation of u_a can only influence the currents on the branches that is directly connected to *a*, so

$$\begin{aligned} i_x &= i_{\text{xa}} + I_{\text{const}(x)} \\ &= -\left(i_{\text{ax}} - \sum_j I_{\text{ax(j)}}\right) + I_{\text{const}(x)} \quad x = b, c, \ldots, m \\ &= -i_{\text{ax}} + \hat{I}_{\text{const}(x)} \end{aligned} \tag{5}$$

where $I_{\text{const}(x)}$ is the summation of currents on branches that directly connected to node *x* except current i_{xa}. $I_{\text{const}(x)}$ will not be influenced by the variation of u_a, so it is constant with the assumption that only u_a can be regulated. With (4) and (5), the derivative of $Pl_{\text{conv}(x)}$ to i_a can be derived as

$$\begin{aligned} \frac{dPl_{\text{conv}(x)}}{di_a} &= \frac{df_x\left(i_x\right)}{di_{\text{ax}}}\frac{di_{\text{ax}}}{di_a} \\ &= -\frac{df_x\left(i_x\right)}{-d\left(-i_{\text{ax}} + \hat{I}_{\text{const}(x)}\right)}\frac{di_{\text{ax}}}{di_a} \quad x = b, c, \ldots, m \\ &= -\frac{df_x\left(i_x\right)}{di_x}\frac{di_{\text{ax}}}{di_a}. \end{aligned} \tag{6}$$

On the other hand, as shown in Fig. 1(b), supposing that there are *k* loads on branch *a*-*x*, the line loss on branch *a*-*x* can be derived as

$$Pl_{\text{line(ax)}} = i_{\text{ax}}^2 R_{\text{ax1}} + \left(i_{\text{ax}} - I_{\text{ax1}}\right)^2 R_{\text{ax2}} + \ldots \quad . \tag{7}$$

So the derivative of $Pl_{\text{line(ax)}}$ to i_a can be derived as

$$\begin{aligned} \frac{dPl_{\text{line(ax)}}}{di_a} &= \frac{dPl_{\text{line(ax)}}}{di_{\text{ax}}}\frac{di_{\text{ax}}}{di_a} \\ &= 2\left(i_{\text{ax}} R_{\text{ax1}} + \left(i_{\text{ax}} - I_{\text{ax1}}\right) R_{\text{ax2}} + \ldots\right)\frac{di_{\text{ax}}}{di_a} \\ &= 2\left(u_a - u_x\right)\frac{di_{\text{ax}}}{di_a}. \end{aligned} \tag{8}$$

Equation (8) shows that, for a certain branch *a*-*x*, the derivative of the line loss ($Pl_{\text{line(ax)}}$) to the current on the branch terminal (i_{ax}) equals twice the voltage drop on the branch ($dPl_{\text{line(ax)}}/di_{\text{ax}} = 2(u_a - u_x)$). This conclusion is the key point that makes the GCM (R_{axj}) and LDM (I_{axj}) ignored in the OPF condition formula.

As (6) and (8), it is important to derive the relationship between di_{ax} and di_a. Fig. 3 shows the equivalent differential circuit of Fig. 1(a). As shown in Fig. 3, in the equivalent differential circuit, all the constant-current sources (loads) are open and all the constant-voltage sources (power supply nodes except *a*) are shorted. So the derivative of i_{ax} to i_a can be derived as

$$\frac{di_{\text{ax}}}{di_a} = \frac{G_{\text{ax}}}{\sum_{j=1}^{m} G_{\text{aj}}} \tag{9}$$

where G_{ax} is the summation of conduction on the branch from *a* to *x*

$$G_{\text{ax}} = \sum \frac{1}{R_{\text{ax}}}. \tag{10}$$

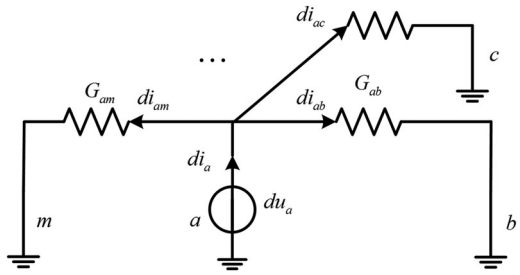

Fig. 3. Equivalent differential circuit of branches directly connected to *a*. Voltage of power supply node *a* is variable while voltages of other power supply nodes is kept constant.

From (3) to (9), the derivative of the gross transmission loss *Pl* to i_a can be derived as

$$\begin{aligned}\frac{dPl}{di_a} &= \sum_{x=a,b,c,\ldots,m} \frac{dPl_{\mathrm{conv}(x)}}{di_a} + \sum_{x=b,c,\ldots,m} \frac{dPl_{\mathrm{line(ax)}}}{di_a} \\ &= \frac{df_a\left(i_a\right)}{di_a} + \sum -\frac{df_x\left(i_a\right)}{di_a}\frac{di_{\mathrm{ax}}}{di_a} + \sum 2\left(u_a - u_x\right)\frac{di_{\mathrm{ax}}}{di_a} \\ &= \left(2u_a + \frac{df_a\left(i_a\right)}{di_a}\right) - \sum_{x=b,c,\ldots,m}\left(2u_x + \frac{df_x\left(i_x\right)}{di_x}\right) \\ &\quad \times \frac{G_{\mathrm{ax}}}{\sum_{j=1}^{m} G_{\mathrm{aj}}}. \end{aligned} \tag{11}$$

For convenience, define $S_j(u_j, i_j)$, namely OPF voltage, as

$$S_j\left(u_j, i_j\right) = u_j + \frac{1}{2}\frac{df_j\left(i_j\right)}{di_j} = u_j + \left(a_j i_j + \frac{1}{2}\mathrm{sign}\left(i_j\right) b_j\right). \tag{12}$$

From (11), when $dPl/di_a = 0$, the transmission loss *Pl* can be minimized. Therefore, to reach the OPF, the operation state of power supply node *a* should be regulated as

$$S_a\left(u_a, i_a\right) = \sum_{x=b,c,\ldots,m} S_x\left(u_x, i_x\right)\frac{G_{\mathrm{ax}}}{\sum_{j=1}^{m} G_{\mathrm{aj}}} \tag{13}$$

where

$$\sum_{x=b,c,\ldots,m} \frac{G_{\mathrm{ax}}}{\sum_{j=1}^{m} G_{\mathrm{aj}}} = 1. \tag{14}$$

C. Derivation of the Global OPF Condition of the Generic DC Microgrid

Equation (13) is the OPF condition of the dc microgrid with the assumption that only u_a can be regulated. With the same derivation extended to all the *X* power supply nodes in the dc microgrid, an *X*-array linear equation group will be obtained

$$\begin{bmatrix} 1 & -k_{\mathrm{ab}} & -k_{\mathrm{ac}} & \ldots & -k_{\mathrm{ax}} \\ -k_{\mathrm{ba}} & 1 & -k_{\mathrm{bc}} & \ldots & -k_{\mathrm{bX}} \\ -k_{\mathrm{ca}} & -k_{\mathrm{cb}} & 1 & \ldots & -k_{\mathrm{cX}} \\ \vdots & \vdots & \vdots & \ddots & \vdots \\ -k_{\mathrm{xa}} & -k_{\mathrm{Xb}} & -k_{\mathrm{Xc}} & \ldots & 1 \end{bmatrix} \begin{bmatrix} S_a \\ S_b \\ S_c \\ \vdots \\ S_X \end{bmatrix} = 0 \tag{15}$$

where

$$k_{\mathrm{xy}} = \frac{G_{\mathrm{xy}}}{\sum_{j\neq x} G_{\mathrm{xj}}} \tag{16}$$

and $G_{\mathrm{xy}} = 0$ if power supply nodes *x* and *y* are not directly connected. So (15) is exactly the extension of (13).

The only solution of (15), which also means the global OPF condition, is

$$S_1\left(u_1, i_1\right) = S_2\left(u_2, i_2\right) = \ldots = S_X\left(u_X, i_X\right). \tag{17}$$

As (12) and (17), only u_j, i_j, a_j, and b_j are included in the derived global OPF condition of a generic structured dc microgrid. u_j and i_j are operation state information of local power supply nodes, which are also necessary in the local converter's primary control. So no extra sensors are needed here to realize the proposed OPF condition. a_j and b_j are converter loss curve (CLC) coefficients of power supply node *j*. The CLC is supposed to be given by the converter's manual or by actual measurements before the converter is connected to the microgrid. None information of grid structure, GCM, nor LDM is necessary.

D. Current Sharing Penalty Term

In a dc microgrid, the proportional current sharing is quite important for the grid's stability and reliability. Commonly, the virtual resistances of droop characters in primary control of power supply nodes are chosen to realize proportional current sharing among the power supply nodes, but if taken the line resistance into consideration, the output current sharing accuracy will be degraded due to the voltage drop across the line [13]. So [13] proposes an improved hierarchical control to enhance the current sharing accuracy.

However, if the microgrid operates in the transmission loss minimization (TLM) state, the current sharing among power supply nodes will be sacrificed. This problem can be solved by adding a current sharing penalty term to the optimal objective function.

Suppose the current sharing target is

$$k_1 i_1 = k_2 i_2 = \ldots = k_x i_x. \tag{18}$$

It can be rewritten as

$$m i_j = \bar{i} \tag{19}$$

where

$$\bar{i} = \frac{\sum_{l=1}^{X} i_l}{X} \tag{20}$$

$$m_j = \frac{k_j \sum_{l=1}^{X} \frac{1}{k_l}}{X}. \tag{21}$$

The optimal objective function (2) can be improved as

$$\begin{cases} \min \quad F = \alpha Pl + (1-\alpha)\sum_{j=1}^{X}\left(m_j i_j - \bar{i}\right)^2 \\ Pl = Pl_{\mathrm{conv}} + Pl_{\mathrm{line}} \\ Pl_{\mathrm{conv}} = \sum Pl_{\mathrm{conv}(x)} = \sum f_x\left(i_x\right) \\ Pl_{\mathrm{line}} = \sum Pl_{\mathrm{line(xy)}} = \sum i_{\mathrm{xy}}^2 R_{\mathrm{xy}} \end{cases} \tag{22}$$

where α is the weight coefficient between transmission power loss and proportional current sharing accuracy. The derivation process in Sections II-B and II-C still fits the new objective function and the TLM with proportional current sharing penalty (TLM-PCS) OPF condition with can be derived as

$$\alpha S_1 + (1-\alpha)\left(m_1 i_1 - \bar{i}\right) = \alpha S_2 + (1-\alpha)\left(m_2 i_2 - \bar{i}\right) = \ldots . \tag{23}$$

If $\alpha = 1$, (23) will degrade into (17), the optimal result leads to TLM operation state of the dc microgrid. On the other hand, if $\alpha = 0$, (23) will degrade into

$$m_1 i_1 - \bar{i} = m_2 i_2 - \bar{i} = \ldots = m_x i_x - \bar{i} \tag{24}$$

which leads to accurate proportional current sharing operation state.

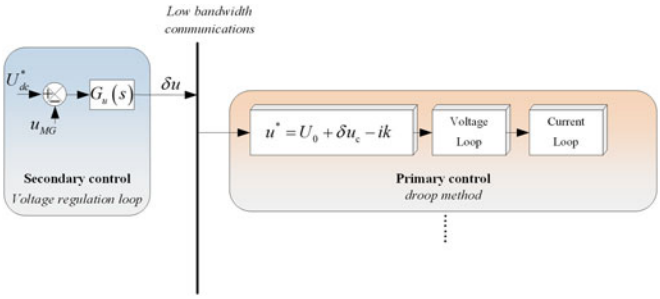

Fig. 4. Conventional hierarchical control of dc microgrid.

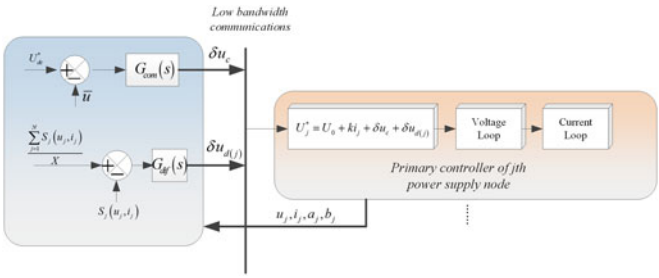

Fig. 5. Control block of the proposed OPF realization method based on hierarchical control.

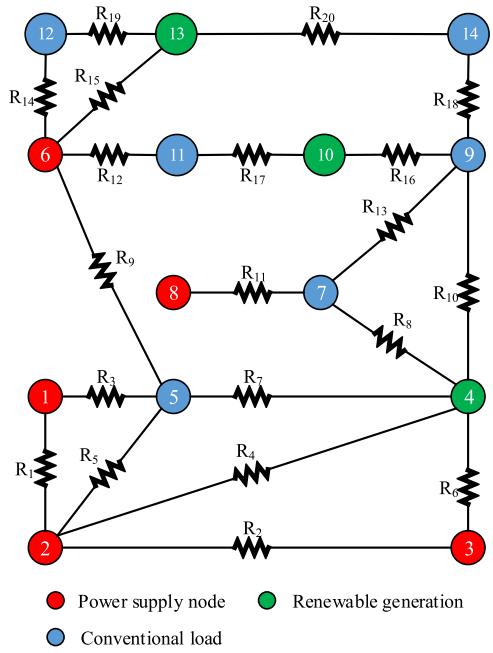

Fig. 6. Modified IEEE 14-bus system for a 400-V dc microgrids OPF testing.

III. OPF Strategy-Based Hierarchical Control for DC Microgrid

In this section, a control strategy based on hierarchical control is proposed to realize the optimal condition shown as (17). Hierarchical control is widely used in dc grids including HVdc, MTDC, and dc microgrids. In the conventional hierarchical control, the primary control layer operates in droop characteristics while the secondary layer aims to restore the voltage deviations produced by the primary droop control [5], shown in Fig. 4.

As shown in Fig. 4, in the conventional hierarchical control, the secondary control layer regulates the microgrid voltage (u_{MG}) by regulating the intercept of the droop characteristics. However, one free degree is actually abandoned in the conventional hierarchical control strategy. As Fig. 4, only a common regulation factor δu is sent from the secondary control layer. So the intercept of droop characteristics in different local converters are always the same as ($u_0 + \delta u$), shown in Fig. 4. Some research has been done by adding a differential regulation factor in the secondary control layer to realize other targets besides the regulation of average voltage. Such as [13], a differential regulation factor is introduced to guarantee the current flow sharing accuracy. In this paper, a differential regulation factor in the secondary control layer is introduced to realization the OPF condition.

To realize the OPF condition in (17), a novel control strategy based on hierarchical control is proposed in Fig. 5. The same with the conventional hierarchical control, the secondary control layer in the proposed control method regulates the microgrid voltage and the power flow in the microgrid by regulating the intercept of droop characteristics in local power supply nodes. Different from the conventional hierarchical control, two regulation factors are sent from the secondary control layer to the primary control layer with low bandwidth communication. δu_c, the common mode regulation factor, aims to regulate the average voltage to the reference just like the conventional hierarchical control. δu_{dj} is the differential mode regulation factor for the realization of OPF condition in (17).

As Fig. 5, in total, there are $(X + 1)$ PI controllers to be calculated in each communication cycle to realize the OPF condition. So the proposed OPF realization method is an $O(n)$ complexity algorithm. Comparing Figs. 4 and 5, the only extra costs of the proposed method are some bandwidth as more data needs to be exchanged and a little more computing resource.

IV. Case Study and Simulation Results

In this section, a series of simulation is done to show the comparison of the proposed method with the conventional hierarchical control and the conventional dc-OPF realization method. To show the improvements of the proposed method, both steady and dynamic performances are compared. The test system in the simulation is based on the IEEE 14-bus system which is introduced in Section IV-A. In Section IV-B, four simulations are done, namely the steady state, load cut off situation, grid reconfiguration situation, and renewable generation variation situation.

A. Test Network and Parameters

To evaluate the proposed OPF condition and hierarchical control method for minimizing the transmission loss, the IEEE 14-bus test system is used. As the test system is designed as an ac power supply grid, the case study here only quotes the grid structure as a generic grid structure, as shown in Fig. 6.

TABLE I
LDM IN THE TEST SYSTEM

Node number	Output/Input Current (A)	Node number	Output/input current (A)
4	59.4440	11	−48.5309
5	−11.2823	12	−64.0425
7	−24.3068	13	32.9938
9	−86.6202	14	−23.6946
10	40.3030		

TABLE II
CONVERTER LOSS COEFFICIENTS OF POWER SUPPLY NODES

Node number	*a*	*b*	*c*
1	0.1964	9.145	51.36
2	0.3681	6.249	23.58
3	0.3455	7.526	41.09
6	0.1571	12.842	99.23
8	0.2182	4.097	15.69

Fig. 6 shows the 400-V dc microgrid structure in the simulation. In the test dc microgrid, nodes 1, 2, 3, 6, 8 are supposed to be power supply nodes as they are all synchronous generators in IEEE 14-bus test system. Nodes 4, 10, 13 are chosen randomly as renewable generation nodes whose output power cannot be regulated. The other nodes are conventional loads.

The GCM is shown set as the same with IEEE 14, while the grid reactance and capacitance are not taken into consideration as they have a little influence on the transmission loss of the dc microgrid.

As the assumptions in Section II, all renewable generation nodes and conventional loads are all taken as load nodes in the OPF analysis and are set as constant-current sources in the simulation tabulated in Table I. In Table I, the input currents are defined as negative and the output currents are positive. As nodes 4, 10, 13 are renewable generation nodes in the simulation, the currents of them are positive.

About the power supply nodes 1, 2, 3, 6, 8, the coefficients of their CLC [*a*, *b*, *c* as (1)] are shown in Table II.

B. Simulation Results

1) Simulation of Steady State: The first simulation is based on a steady situation when the grid structure (see Fig. 6) and the load distribution (see Table I) are hold still. The operation states of power supply nodes in the grid by different control methods are listed in Table III. In Table III, the theoretical OPF condition is obtained by the conventional dc-OPF algorithm [2]

$$\min f\left(\vec{V},\vec{i}\right)=\sum_{i=1}^{N}\sum_{j=i+1}^{N}G_{\mathrm{ij}}\left(V_i-V_j\right)^2+\sum_{k=1,2,3,6,8}f_k\left(i_k\right)$$

$$\text{cons.}\begin{cases} i_k=\sum\limits_{j\neq k}G_{\mathrm{kj}}\left(V_k-V_j\right) \\ i_k=I_k \quad k\neq 1,2,3,6,8 \\ V_{\mathrm{ave}}=\sum\limits_{i=1}^{N}V_i/N=V_{\mathrm{ref}}. \end{cases} \tag{25}$$

TABLE III
POWER SUPPLY NODES OUTPUT VOLTAGE WITH DIFFERENT CONTROL METHODS

Node number	OPERATION STATE	Theoretical OPF condition	Conventional OPF realization	Proposed OPF realization (see Fig. 5)
1	Output voltage (V)	401.8587	401.8732	401.8447
2	Output voltage (V)	401.7261	401.7392	401.7107
3	Output voltage (V)	401.8861	401.8969	401.8665
6	Output voltage (V)	400.8439	400.8550	400.8267
8	Output voltage (V)	400.9871	400.9981	400.9697
	Gross converter loss (W)	1988.3571	1988.1894	1988.2285
Test grid	Gross line loss (W)	531.3659	532.0046	533.2875
	Gross transmission loss (W)	2519.7230	2520.1940	2521.5160

In (25), G_{kj} is the line conductance of branch *k-j* which contains information of GCM, I_k contains the LDM (see Table I) and (a_k, b_k, c_k) is the CLC coefficients (see Table II).

The solution of the optimization problem (as shown in (25)) can be obtained by solving its Largrangian derivative [2], which is commonly used in the conventional OPF algorithm for both ac grids and dc grids. So it would be an $N \times N$ (N is the number of nodes and $N = 14$ in this case) matrixes iteration process to solve the problem ($O(n^2)$ complexity). As analyzed in Section III, the proposed OPF realization method is an $O(n)$ algorithm whose complexity is increased with the number of power supply nodes ($X = 5$ in this case) in the grid. Equation (25) is also used in the secondary control layer of the conventional OPF realization method.

Although both OPF conditions obtained by conventional OPF realization method and proposed OPF realization method are accurate, as Table III, it is difficult to keep the outputs of the power supply nodes (with power electronics converters) exactly at the OPF condition because of the ripples on both output voltages and currents of power supply nodes. So the transmission losses of both methods are a little higher than the theoretical minimized value. For the proposed OPF realization method, the actual transmission loss deviates further from the theoretical minimized value, because the ripples on the outputs of the power supply nodes also influence the sampling of the output voltages and output currents of the power supply nodes which will further influence the accuracy of the OPF realization in the secondary control layer in Fig. 5. On the other hand, the conventional OPF realization method obtains the OPF condition by solving the optimization problem as (25), so the output ripples will not influence its OPF algorithm.

Though influenced by the output ripples, performances of both OPF realization methods are quite close to the theoretical OPF condition while the transmission loss of the conventional hierarchical method is relatively much higher, which proves the benefits of OPF realization.

2) OPF With Current Sharing Penalty Term: In order to verify the TLM-PCS tradeoff OPF strategy proposed in Section II-D, simulation is done based on the OPF condition shown as (23). The current sharing target of the power supply nodes is set

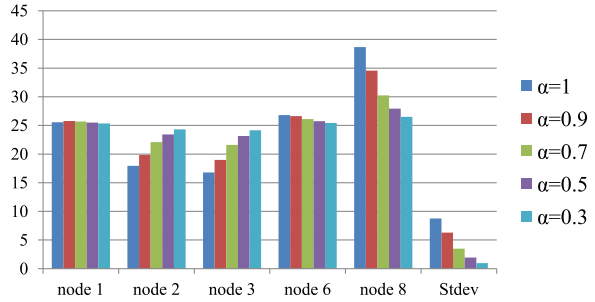

Fig. 7. Proposed TLM-PCS OPF current sharing accuracy.

TABLE IV
TRANSMISSION LOSS WITH THE PROPOSED TLM-PCS OPF

Weight coefficient (α)	GROSS LINE LOSS (W)	Gross converter loss (W)	Gross transmission loss (W)
1	533.2875	1988.2285	2521.5160
0.9	548.6272	1997.8960	2546.5232
0.7	557.9614	2052.9403	2610.9017
0.5	563.5948	2118.6557	2682.2505
0.3	577.365	2181.5149	2758.8799

as $i_1 = i_2 = i_3 = i_6 = i_8$. The simulation results are shown as Fig. 7 and Table IV.

As Fig. 7 and Table IV, with the weight coefficient α change from 1 to 0.3, the standard deviation (Stdev) of the output currents of the five power supply nodes reduces from 8.732 to 0.962 A but the transmission loss rises from 2521 to 2758 W. This simulation proves that the proposed TLM-PCS OPF strategy [see (23)] is effective to keep the balance between current sharing accuracy and TLM.

3) Load Cut Off Situation: In this simulation, the test system is first operating with the load distribution shown in Table I and at $t = 1$ s, the load on Node 9 (randomly chosen) is cut off. Fig. 8 shows the simulation results. In Fig. 8, the transmission loss is the sum of all converter losses and line losses and the dc bus voltage is the average voltage of all nodes.

As one load is cut off, the theoretical minimized value of the transmission loss steps from 2519.72 to 1101.48 W. It takes both the proposed OPF realization control method and the conventional OPF realization control method a few communication cycles (0.1 s) to regulate the system to the new OPF condition. As the conventional OPF method is based on the prior information of the grid and load information, the regulation of conventional OPF method is relatively faster than the proposed one. However, even though the proposed method can only get the information of the operation states and CLCs of the power supply nodes (see Table II), it can still regulate the entire system to the OPF condition. The situation is quite the same in the regulation of the dc bus voltage. With all the information available, the conventional OPF realization method regulates the dc voltage bus faster with smaller deviation but the proposed method can also restore the deviation of the dc bus voltage caused by the load cut off, just with a few more communication cycles. On the other hand, the dynamic responses of the microgrid voltage

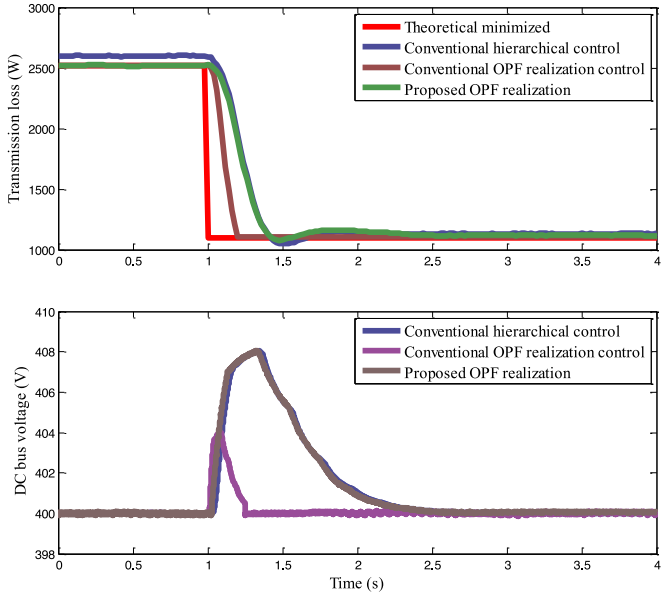

Fig. 8. Simulation results of load cut off situation. Load on Node 9 is cut off at $t = 1$ s.

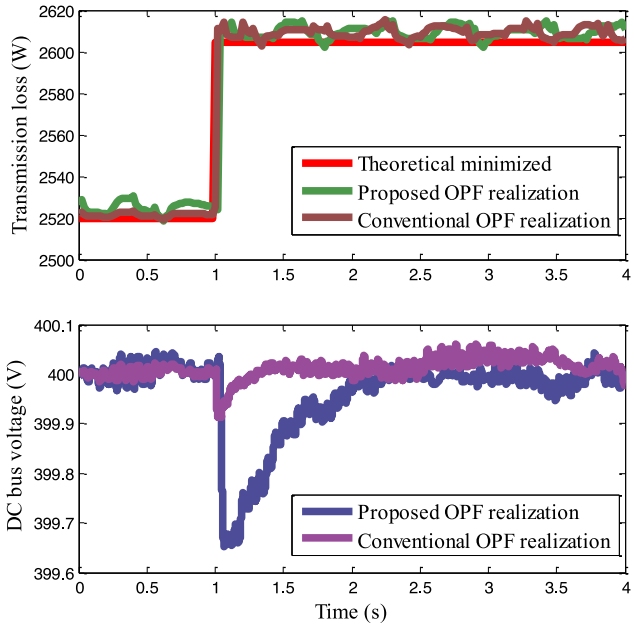

Fig. 9. Simulation results of grid reconfiguration situation. Branch 6–11 is broken at $t = 1$ s.

of the proposed OPF realization method and the conventional hierarchical control are almost the same, which means the proposed OPF realization method can realize the dc microgrid OPF condition without sacrificing the dc voltage regulation function of the conventional hierarchical control.

4) Grid Reconfiguration Situation: In this simulation, the grid structure is set as Fig. 6 at the beginning and branch 6–11 is broken at $t = 1$ s. So the grid structure is reconfigured. Fig. 9 shows the simulation results.

As shown in Fig. 9, the derivation of the dc bus voltage is much smaller than that in Fig. 8 because the grid reconfiguration will

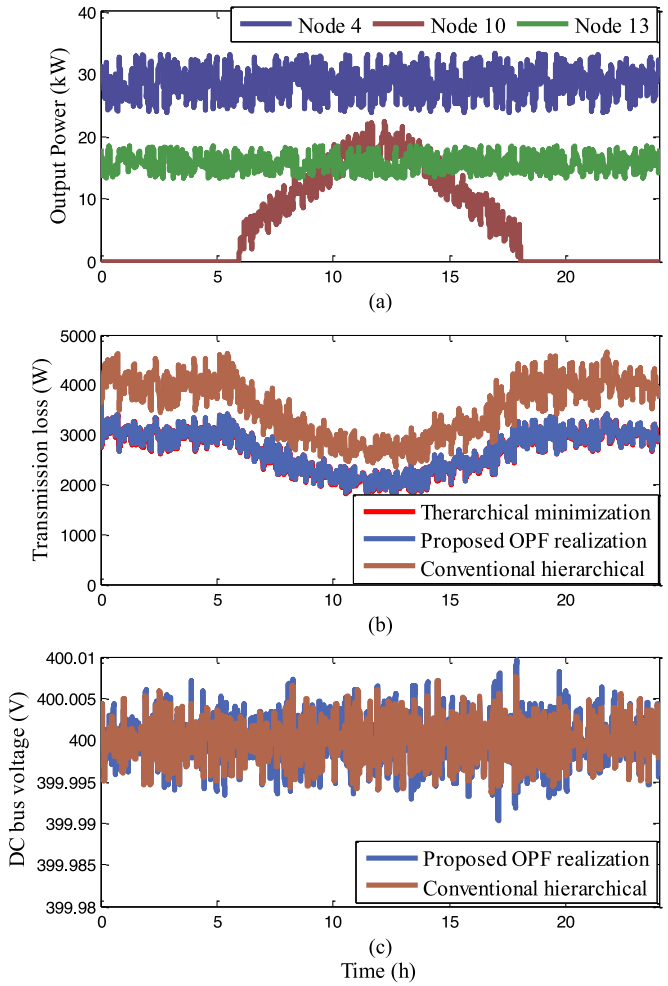

Fig. 10. Simulation results of renewable energy variation situation. (a) Output current of Node 13; (b) transmission loss and dc bus voltage of the grid.

not break the power balance in the test system. So the dc bus voltage deviation is much smaller than the load cut off situation. The same with the load cut off situation, the response speed of the conventional realization method is faster but both methods can restore the voltage deviation and realize the OPF condition at the same time.

5) Renewable Energy Randomness Influence: In this simulation, the validity of the proposed OPF realization method is tested under different sort of renewable sources dynamic challenges. In the simulation, node 10 is connected to a PV generation while node 4 and 13 are connected to wind turbines. To be more realistic, the simulation time is set to 24 h. The PV node generates power only in day time and all renewable energy sources' generation is stochastic. The output power of the three renewable energy sources is shown as Fig. 10(a). Fig. 10(b) and (c) prove that the randomness of renewable energy sources has little influence on the efficiency of the proposed OPF realization method. The simulation result also shows that the proposed OPF reduces the transmission loss by 24.3% comparing with conventional hierarchical control and the transmission efficiency is raised by 0.83%. 20.6-kW·h electric power is saved during a day.

TABLE V
POWER SUPPLY NODES OUTPUT VOLTAGE WITH DIFFERENT CONTROL METHODS

	Conventional OPF Realization	Proposed OPF realization	Conventional hierarchical control
Functions	OPF; Voltage regulation	OPF; Voltage regulation	Voltage regulation
OPF accuracy	Accurate	Accurate	×
Computational complexity	$N \times N$ matrixes iteration $O(n^2)$	$(X+1)$ PI controllers $O(n)$	One PI controller only
Transmission loss deviation from the theoretical minimization	0.187%	0.712%	3.1%
Response speed (communication cycles)	1–2	10	10
Information required	GCM; LDM; CLC;	CLC; Operation states; Grid voltages	Grid voltages
Transmission efficiency	97.41%	97.40%	96.57%

With the four simulations introduced in Section IV-B, the comparison of the conventional OPF realization method and the proposed realization method can be drawn as Table V.

As Table V, the transmission loss with the proposed OPF realization method is a little larger and the response speed is slower than the conventional OPF realization method, but the shortcoming is far away from intolerant. On the other hand, the simulations also prove that the proposed method can fulfil the OPF task in variable situations (load cut off, grid reconfiguration, and smoothly changing renewable energy generation) without any extra information of the grid. In an actual dc microgrid, there may be frequent load variation, grid reconfiguration, and energy generation variation during the operation. The conventional OPF realization method can hardly be realized. Actually, the conventional dc-OPF is mainly used in HVdc or MTDC with the grid that has relatively finite nodes and is rarely changed. Take the expansibility and economic efficiency into consideration, the proposed OPF realization method is far more efficient and feasible than the conventional one.

V. EXPERIMENTAL RESULTS

In this section, experimental results of the proposed OPF condition and hierarchical control method are introduced. In part Section V-A, the experimental platform is introduced. Then, the proposed approach is verified by experiments with two steps. Section V-B proves that the minimized transmission loss condition derived in Section II is the global OPF condition of the transmission loss. Section V-C verifies the validity of the proposed method in Section III.

A. Experimental Platform

As Fig. 11, a 50-V dc microgrid experimental platform is established to verify the proposed OPF strategy. The proto grid contains two power supply nodes which are connected to the dc bus with two boost converters and one load node (a rheostat).

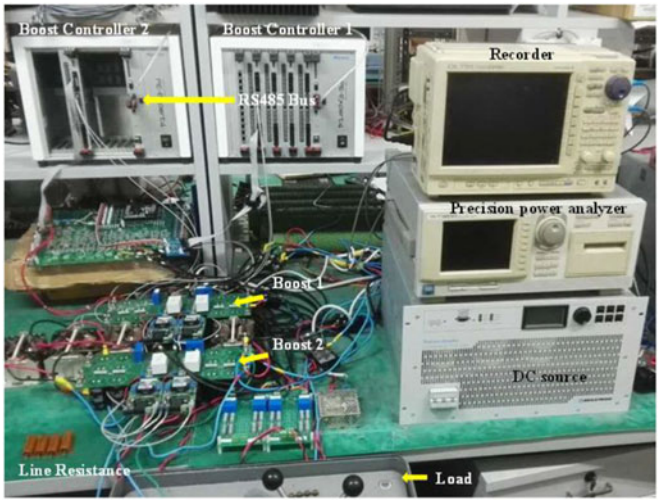

Fig. 11. Experimental platform.

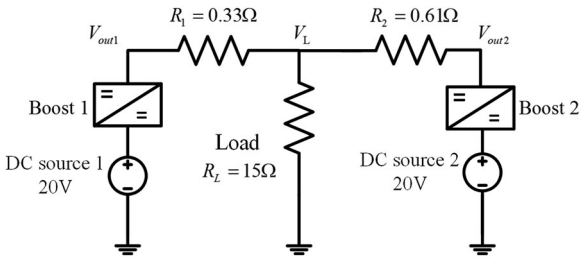

Fig. 12. Experimental platform grid parameters.

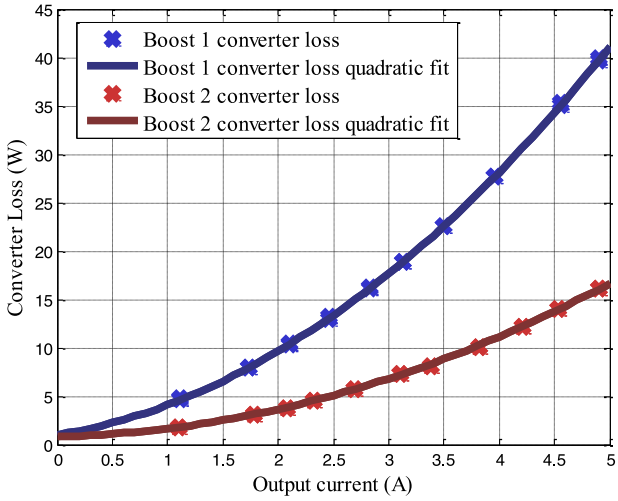

Fig. 13. Converter loss modeling and the quadratic fitting results of the two boost converters.

Some precision resistances are utilized as the line resistance. Two power electronics controllers (Myway, PE-Expert 4) are utilized as the boosts' controllers. Communication between the two controllers is realized by RS 485 bus. The line losses and converter losses of each part are measured by the precision power analyzer (YOKOGAWA, WT1600). The output voltage of the dc source is 20 V and the line impedance and load distribution are shown in Fig. 12.

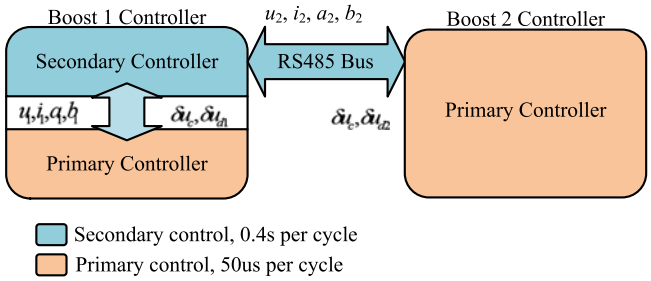

Fig. 14. Control strategy of the experimental platform.

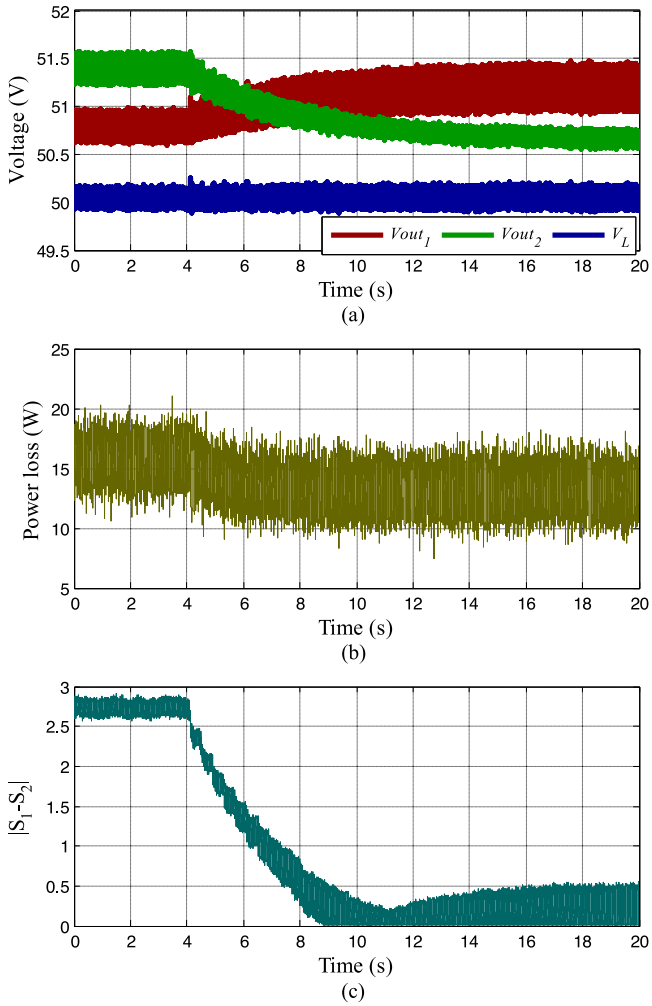

Fig. 15. Comparison of conventional hierarchical control with proposed control method in transmission power loss. The system operates with conventional hierarchical control at start and switches to proposed control method at $t = 4$ s.

In order to implement the OPF strategy, the CLC of the two boosts should first be measured and quadratic fitted in order to obtain the converter loss parameters, as shown in Fig. 13.

The control strategy to implement the proposed OPF hierarchical control is shown as Fig. 14. The secondary control layer is embedded in Boost 1 controller. The secondary controller updates the operation information of Boost 2 by RS 485

TABLE VI
COMPARISON OF CONVENTIONAL HIERARCHICAL CONTROL AND THE PROPOSED CONTROL

		Conventional hierarchical control	Proposed hierarchical control
Converter loss	Boost 1	8.09 W	6.65 W
	Boost 2	3.19 W	2.19 W
Line loss	R_1	2.39 W	3.50 W
	R_2	1.48 W	0.50 W
Transmission efficiency		91.66%	92.83%

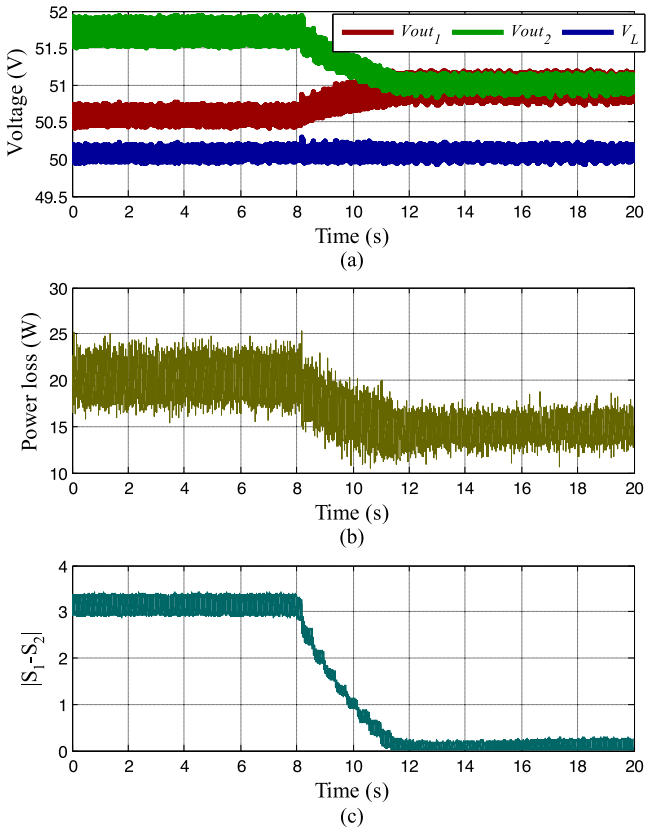

Fig. 16. Comparison of conventional hierarchical control with the proposed control method in transmission power loss. $R_1 = 0.22\ \Omega$, $R_2 = 0.81\ \Omega$.

communication and executes the secondary control every 0.4 s while the primary controllers operate in droop mode.

B. Experiments of the Proposed Hierarchical Control

To verify the validity of the proposed hierarchical control method, Fig. 15 shows the control mode switch from the conventional hierarchical control to the proposed OPF hierarchical control. In Fig. 15, the secondary control layer in operating with the conventional control method (see Fig. 4) is and switches to the proposed method (see Fig. 5) at $t = 4$ s.

Detailed transmission losses comparison is shown in Table VI. As Table VI, the entire transmission loss drops from 15.17 to 12.87 W after the control mode switch from conventional hierarchical control to the proposed one and the differential of S_1 and S_2 is regulated to 0. The communication cycle

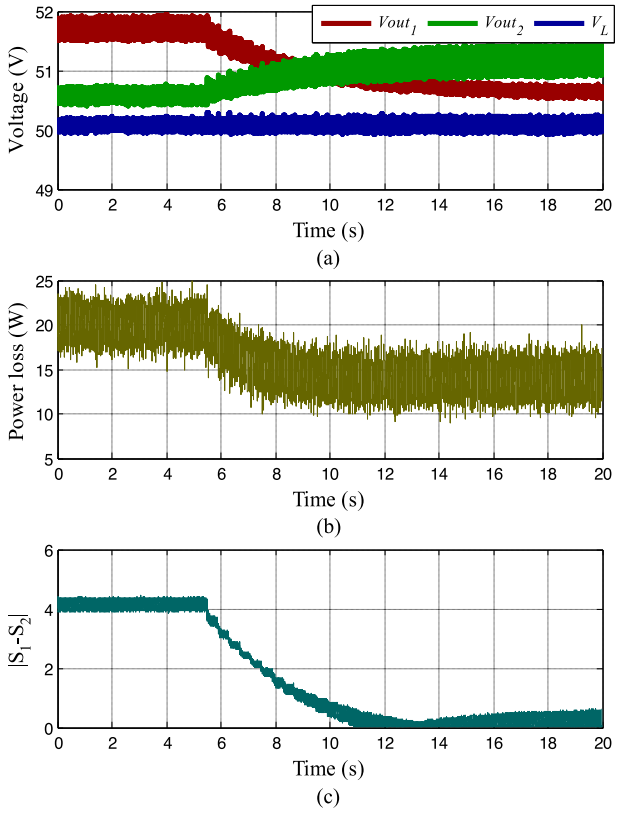

Fig. 17. Comparison of conventional hierarchical control with the proposed control method in transmission power loss. $R_1 = 0.81\ \Omega$, $R_2 = 0.22\ \Omega$.

TABLE VII
TRANSMISSION LOSSES COMPARISON ($R_1 = 0.22\ \Omega$, $R_2 = 0.81\ \Omega$)

		Conventional hierarchical control	Proposed hierarchical control
Converter loss	Boost 1	11.83	5.79
	Boost 2	3.21	5.80
Line loss	R_1	4.80	1.48
	R_2	0.52	1.68
Transmission efficiency		89.11%	91.86%

TABLE VIII
TRANSMISSION LOSSES COMPARISON ($R_1 = 0.81\ \Omega$, $R_2 = 0.22\ \Omega$)

		Conventional hierarchical control	Proposed hierarchical control
Converter loss	Boost 1	11.83	5.79
	Boost 2	3.21	5.80
Line loss	R_1	4.80	1.48
	R_2	0.52	1.68
Transmission efficiency		89.11%	91.86%

in the experiment is 0.4 s, which means it takes the secondary layer 10–15 cycles to regulate the whole system to the TLM condition.

Some more similar experiments are done with different line resistances. The results are show as Figs. 16 and 17. Detailed

transmission losses comparison results of the two experiments are shown in Tables VII and VIII.

VI. Conclusion

In this paper, an OPF strategy for dc microgrids based on hierarchical control is proposed to minimize the transmission loss in a generic dc microgrid. Both converter loss and ohmic line loss are taken into consideration. The proposed control strategy is based on the local information of power supply nodes in the microgrid and none of prior knowledge of grid structure, GCM, and LDM is needed. The proposed method is verified with both simulation and experiment. Simulation results show that the proposed method can realize both dc bus voltage regulation and OPF condition at the same time in both steady and dynamic situations. Though the response speed of the proposed method is slower than the conventional dc-OPF realization method and the dc bus voltage deviation is larger, the feasibility, extensibility, and economic efficiency are much higher than the conventional method. The experimental results prove the proposed OPF condition by a global search of the proto system and verify the proposed method by a control mode switch experiment from conventional hierarchical control to the proposed one. The transmission loss drops 15% with the control mode switch. Both simulation and experiment prove that the proposed method can realize both the OPF condition and the microgrid voltage regulation of generic dc microgrids without information of GCM and LDM.

References

[1] M. Aragüés-Peñalba, A. Egea-Àlvarez, O. Gomis-Bellmunt, and A. Sumper, "Optimum voltage control for loss minimization in HVDC multi-terminal transmission systems for large offshore wind farms," *Electr. Power Syst. Res.*, vol. 89, pp. 54–63, 2012.

[2] K. Rouzbehi, A. Miranian, A. Luna, and P. Rodriguez, "DC voltage control and power sharing in multiterminal DC grids based on optimal DC power flow and voltage-droop strategy," *IEEE J. Emerg. Sel. Topics Power Electron.*, vol. 2, no. 4, pp. 1171–1180, Dec. 2014.

[3] J. Cao, W. Du, H. F. Wang, and S. Q. Bu, "Minimization of transmission loss in meshed AC/DC grids with VSC-MTDC networks," *IEEE Trans. Power Syst.*, vol. 28, no. 3, pp. 3047–3055, Aug. 2013.

[4] A. Changsun and P. Huei, "Decentralized voltage control to minimize distribution power loss of microgrids," *IEEE Trans. Smart Grid*, vol. 4, no. 3, pp. 1297–1304, Sep. 2013.

[5] J. M. Guerrero, J. C. Vasquez, J. Matas, L. G. De Vicuna, and M. Castilla, "Hierarchical control of droop-controlled AC and DC microgrids—A general approach toward standardization," *IEEE Trans. Ind. Electron.*, vol. 58, no. 1, pp. 158–172, Jan. 2011.

[6] D. Boroyevich, I. Cvetkovic, R. Burgos, and D. Dong, "Intergrid: A future electronic energy network?" *IEEE J. Emerg. Sel. Topics Power Electron.*, vol. 1, no. 3, pp. 127–138, Sep. 2013.

[7] J. Chi, W. Peng, X. Jianfang, T. Yi, and H. C. Fook, "Implementation of hierarchical control in DC microgrids," *IEEE Trans. Ind. Electron.*, vol. 61, no. 8, pp. 4032–4042, Aug. 2014.

[8] T. Dragicevic, J. M. Guerrero, J. C. Vasquez, and D. Skrlec, "Supervisory control of an adaptive-droop regulated DC microgrid with battery management capability," *IEEE Trans. Power Electron.*, vol. 29, no. 2, pp. 695–706, Feb. 2014.

[9] Q. Shafiee, T. Dragicevic, J. C. Vasquez, and J. M. Guerrero, "Hierarchical control for multiple DC-microgrids clusters," *IEEE Trans. Energy Convers.*, vol. 29, no. 4, pp. 922–933, Dec. 2014.

[10] Y. Xunwei, S. Xu, N. Xijun, and A. Q. Huang, "System integration and hierarchical power management strategy for a solid-state transformer interfaced microgrid system," *IEEE Trans. Power Electron.*, vol. 29, no. 8, pp. 4414–4425, Aug. 2014.

[11] M. Sechilariu, W. Baochao, and F. Locment, "Building integrated photovoltaic system with energy storage and smart grid communication," *IEEE Trans. Ind. Electron.*, vol. 60, no. 4, pp. 1607–1618, Apr. 2013.

[12] L. Xiaonan, S. Kai, J. M. Guerrero, J. C. Vasquez, and H. Lipei, "State-of-charge balance using adaptive droop control for distributed energy storage systems in DC microgrid applications," *IEEE Trans. Ind. Electron.*, vol. 61, no. 6, pp. 2804–2815, Jun. 2014.

[13] L. Xiaonan, J. M. Guerrero, S. Kai, and J. C. Vasquez, "An improved droop control method for DC microgrids based on low bandwidth communication with DC bus voltage restoration and enhanced current sharing accuracy," *IEEE Trans. Power Electron.*, vol. 29, no. 4, pp. 1800–1812, Apr. 2014.

[14] J. Beerten, S. Cole, and R. Belmans, "Generalized steady-state VSC MTDC model for sequential AC/DC power flow algorithms," *IEEE Trans. Power Syst.*, vol. 27, no. 2, pp. 821–829, May 2012.

[15] J. Xiao, P. Wang, and L. Setyawan, "Hierarchical control of hybrid energy storage system in DC microgrids," *IEEE Trans. Ind. Electron.*, vol. 62, no. 8, pp. 4915–4924, Aug. 2015.

[16] A. Rabiee and A. Soroudi, "Stochastic multiperiod OPF model of power systems with HVDC-connected intermittent wind power generation," *IEEE Trans. Power Del.*, vol. 29, no. 4, pp. 336–344, Jul. 2014.

[17] W. Wang and M. Barnes, "Power flow algorithms for multi-terminal VSC-HVDC with droop control," *IEEE Trans. Power Syst.*, vol. 29, no. 4, pp. 1721–1730, Jul. 2014.

[18] E. Iggland, R. Wiget, S. Chatzivasileiadis, and G. Anderson, "Multi-area DC-OPF for HVAC and HVDC grids," *IEEE Trans. Power Syst.*, vol. 30, no. 5, pp. 2450–2459, Sep. 2015.

[19] M. Hosseinzadeh and F. R. Salmasi, "Robust optimal power management system for a hybrid AC/DC micro-grid," *IEEE Trans. Sustainable Energy*, vol. 6, no. 3, pp. 675–687, Jul. 2015.

[20] M. Baradar, M. R. Hesamzadeh, and M. Ghandhari, "Second-order cone programming for optimal power flow in VSC-type AC-DC grids," *IEEE Trans. Power Syst.*, vol. 28, no. 4, pp. 4282–4291, Nov. 2013.

[21] J. Liang, T. Jing, O. Gomis-Bellmunt, J. Ekanayake, and N. Jenkins, "Operation and control of multiterminal HVDC transmission for offshore wind farms," *IEEE Trans. Power Del.*, vol. 26, no. 4, pp. 2596–2604, Oct. 2011.

Junchao Ma (S'13) received the B.S. degree in electrical engineering from Xi'an Jiaotong University, Xi'an, China, in 2011. He is currently working toward the Ph.D. degree in electrical engineering at the State Key Laboratory of Power System, Tsinghua University, Beijing, China.

His research interests include renewable energy generation and dc microgrid.

Liqiang Yuan (M'02) received the B.S. and Ph.D. degrees from Tsinghua University, Beijing, China, in 1999 and 2004, respectively.

He is currently an Associate Professor with the Department of Electrical Engineering, Tsinghua University. His research interests include photovoltaic power systems and solid-state transformer.

Zhengming Zhao (M'02–SM'03) received the B.S. and M.S. degrees in electrical engineering from Hunan University, Changsha, China, in 1982 and 1985, respectively, and the Ph.D. degree from Tsinghua University, Beijing, China, in 1991.

In 1991, he joined the Department of Electrical Engineering, Tsinghua University. From 1994 to 1996, he was a Postdoctoral Fellow with The Ohio State University, Columbus, OH, USA, and then was a Visiting Scholar with the University of California, Irvine, CA, USA, for one year. He is currently a Professor with the Department of Electrical Engineering and the Deputy Director of the State Key Laboratory of Power System, Tsinghua University. His research interests include high-power conversion, power electronics and motor control, and solar energy applications.

Prof. Zhao is a Fellow of the Institution of Engineering and Technology, U.K. He is also the Vice President of the Beijing Power Electronics Society and the Chairman of the IEEE Power Electronics Society Beijing Chapter.

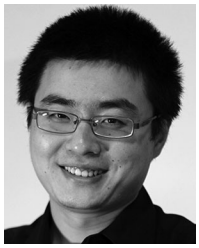

Fanbo He (M'12) received the B.S. and Ph.D. degrees in electrical engineering from Tsinghua University, Beijing, China, in 2007 and 2012, respectively.

He is currently with the Institute for Energy Internet Research, Tsinghua University. His research interests include photovoltaic power systems and wireless power transfer.